Journal of Medicinal Chemistry

Article

A TREK Channel Family Activator with Well-Defined Structure-Activation Relationship for Pain and Neurogenic Inflammation

Yunguang Qiu, Lu Huang, Jie Fu, Chenxia Han, Jing Fang, Ping Liao, Zhuo Chen, Yiqing Mo, Peihua Sun, Daqing Liao, Linghui Yang, Jing Wang, qiansen zhang, Jin Liu, Feng Liu, Tingting Liu, Wei Huang, Huaiyu Yang, and Ruotian Jiang

J. Med. Chem., **Just Accepted Manuscript** • DOI: 10.1021/acs.jmedchem.9b02163 • Publication Date (Web): 12 Mar 2020

is published by the American Chemical Society. 1155 Sixteenth Street N.W., Washington, DC 20036

A TREK Channel Family Activator with Well-Defined Structure-Activation Relationship for Pain and Neurogenic Inflammation

Yunguang Qiu[†,§,¶,#], Lu Huang[‡,#], Jie Fu[†,#], Chenxia Han[//], Jing Fang[⊥], Ping Liao[‡], Zhuo Chen[‡], Yiqing Mo[†], Peihua Sun[⊥], Daqing Liao[‡], Linghui Yang[‡], Jing Wang[‡], Qiansen Zhang[†], Jin Liu[‡], Feng Liu[⊥], Tingting Liu[//], Wei Huang[//], Huaiyu Yang[†,] and Ruotian Jiang[‡,*]*

[†]Shanghai Key Laboratory of Regulatory Biology, Institute of Biomedical Sciences, School of Life Sciences, East China Normal University, Shanghai 200241, China.

[‡]Laboratory of Anesthesia and Critical Care Medicine, National-Local Joint Engineering Research Center of Translational Medicine of Anesthesiology, West China Hospital, Sichuan University & The Research Units of West China (2018RU012), Chinese Academy of Medical Sciences, Chengdu 610000, China.

[§]State Key Laboratory of Drug Research and CAS Key Laboratory of Receptor Research, Shanghai Institute of Materia Medica, Chinese Academy of Sciences, Shanghai 201203, China.

[∥]Department of Integrated Traditional Chinese and Western Medicine, Sichuan Provincial Pancreatitis Centre and West China-Liverpool Biomedical Research Centre, West China Hospital, Sichuan University, Chengdu 610000, China

[⊥]Jiangsu Key Laboratory of Neuropsychiatric Diseases and College of Pharmaceutical Sciences, Soochow University, Suzhou 215123, China

[¶]University of Chinese Academy of Sciences, Beijing 100049, China

ABSTRACT. TWIK-related K^+ (TREK) channels are potential analgesic targets. However, selective activators for TREK with both defined action mechanism and analgesic ability for chronic pain have been lacking. Here we report C3001a, a selective activator for TREK against other two-pore domain K^+ (K2P) channels. C3001a binds to the cryptic binding site formed by P1 and TM4 in TREK-1, as suggested by computational modeling and

experimental analysis. Further, we identify the carboxyl group of C3001a as a structural determinant for the binding to TREK-1/2, and the key residue that defines the subtype-selectivity of C3001a. C3001a targets TREK channels in peripheral nervous system to reduce the excitability of nociceptive neurons. In neuropathic pain, C3001a alleviated spontaneous pain and cold hyperalgesia. In a mouse model of acute pancreatitis, C3001a alleviated mechanical allodynia and inflammation. Together, C3001a represents a lead compound which could advance the rational design of peripherally-acting analgesics targeting K2P channels without opioid-like adverse effects.

INTRODUCTION

Long-term opioid administration has minimal effects on chronic pain and is generally coupled with tolerance, dependence, and addiction[1]. In acute pancreatitis (AP), the use of morphine for pain control may even exacerbate the disease by increasing pancreatic neutrophilic infiltration and necrosis[2]. Thus, there is a clinically unmet demand for developing new non-opioid analgesics. In this regard, the two-pore domain K^+ (K2P) channels are considered as emerging candidates[3, 4]. Recently, we showed that activation

of the TWIK-related acid-sensitive K^+ 3 (TASK-3) channel, a K2P channel, using a newly discovered selective activator CHET3, displayed therapeutic potential in analgesia[5]. K2P family channels consist of 15 gene products, and each of those contains four transmembrane segments (TM1–TM4) and two-pore domains (P1 and P2)[6]. In the K2P family, the TWIK-related K^+ channel (TREK) subfamily is comprised of TREK-1 (*Kcnk2*), TREK-2 *(Kcnk10*), and TWIK-related arachidonic acid-stimulated K^+ channel (TRAAK, *Kcnk4*). The TREK family channels share >78% sequence homology and some common activation mechanisms[7]. They are mechanical-, thermal- and lipid-gated channels that can be regulated by different physical and chemical stimuli, including membrane stretch[8, 9], membrane depolarization[10], temperature[11], pH[12, 13], arachidonic acid, and other polyunsaturated fatty acids[9]. In peripheral sensory neurons, TREK-1 is expressed in peptidergic substance P (SP)-positive fibers or nonpeptidergic isolectin 4-positive ($IB4^+$) C-fibers and co-localized with transient receptor potential cation channel subfamily V member 1 (TRPV1) channels[14], while TREK-2 is selectively expressed in $IB4^+$ C-fibers[15]. Functionally, TREK channels produce background K^+ currents which contribute to the resting membrane potential (RMP) and action potential properties of nociceptive

neurons[16]. A recent study by Kanda et al[17] found that TREK-1 and TRAAK are highly enriched at the nodes of Ranvier of trigeminal myelinated afferent nerves, in which they mediate rapid action potential conduction and are involved in sensory behavioral response. TREK-1, TREK-2 or TRAAK knockout mice showed significantly increased sensitivity to mechanical and thermal stimuli[14, 18, 19]. Notably, Devilliers et al[20] found that morphine may enhance the TREK-1-mediated currents by phosphorylating the channel, and the enhancement of TREK-1 function contributes to the analgesic effect of morphine without its adverse side effects. Thus, activation of TREK channels may provide an opportunity to dissociate the analgesic from major adverse effects of opioids for pain therapies.

A few compounds have been previously identified that selectively activate TREK channels including ML67-33, BL-1249, ML335, ML402, and GI-530159[21-24]. However, to our knowledge, except for a derivative of BL-1249[25], the pharmacokinetic profiles as well as the in vivo ability of these compounds remain largely unreported. So far, the selective TREK-1 activators with reported in vivo analgesic properties are cinnamyl 3,4-dihydroxyl-

α-cyanocinnamate analogues derived from caffeate esters[26]. However, the binding site and the molecular basis for the subtype-selectivity of these compounds in TREK channels are unclear. It is noteworthy that under chronic pain conditions, the expression of TREK channels was downregulated[18, 27, 28]. Therefore, whether selective activation of TREK channels is sufficient to attenuate thermal hyperalgesia and mechanical allodynia under chronic pain remains to be determined. In the search of small molecules with new chemical scaffolds, which selectively activate TREK channels, we discovered a subtype-selective TREK-1/2 activator, (1*S*,3*R*)-3-((4-(6-methylbenzo[*d*]thiazol-2-yl)phenyl)carbamoyl)cyclopentane-1-carboxylic acid (named C3001a). Using computational and experimental methods, we defined the binding mode and the structural selectivity basis of C3001a in TREK-1. Having characterized the inhibitory role of C3001a in the excitability of nociceptive neurons, we further explored the therapeutic potential of C3001a in mouse models for inflammatory or neuropathic pain. Particularly, since the tight coupling between TREK-1 and μ-opioid receptor (μOR), we evaluated the therapeutic effects of activation of TREK channels by C3001a in a mouse model of AP.

AP in mice represents a specific preclinical visceral inflammatory pain model in which the opioids have debatable therapeutic application[2, 29].

RESULTS

C3001a selectively activates TREK channels, preferentially TREK-1 and TREK-2 channels. In one of our in-house experimental screenings performed to find bioactive compounds for the TREK-1, we identified C3001a (Figure 1A) as a potential TREK-1 activator. In the whole-cell voltage clamp experiments on human embryonic kidney (HEK)-293T cells that were transiently transfected with recombinant human TREK-1, increase in current amplitude was recorded by the extracellular application of C3001a, and the increase could be rapidly reversed by washout (Figure 1B). The effect of C3001a in increasing the current was concentration-dependent with a half-maximum effective concentration (EC_{50}) of 12.81 μM (Figure 1C). To further verify that C3001a is indeed an activator of TREK-1, we tested C3001a on TREK-1 channels using inside-out and outside-out patches. The outside-out recordings revealed that C3001a significantly increased the open probability of TREK-1 (P = 0.0058 for -60 mV, P = 0.0054 for +60

mV), with no change in single channel conductance (P = 0.486 for -60 mV, P = 0.055 for +60 mV Figure 1D-G). Interestingly, C3001a did not show any significant effects on the open probability or channel conductance of TREK-1 in the inside-out recordings (Figure S1). Thus, the single channel recordings suggest that C3001a directly activates TREK-1 through a binding site accessible from the extracellular side of TREK-1. We further investigated whether C3001a also activates other K2P channels. TREK-2 and TRAAK, two other TREK subfamily members, responded to C3001a with similar EC_{50} (11.31 μM and 15.29 μM, respectively). C3001a activated TREK-2 with relatively high efficacy (~4.5-fold at 10 μM in comparison to control) which was similar to that on TREK-1. However, C3001a activated TRAAK with relatively low efficacy (~2.4-fold at 10 μM in comparison to control) (Figure. 1H and Figure S2). C3001a showed little effects on other human K2P channels, including TWIK-related acid-sensitive K^+ 3 (TASK-3), TASK-1, TWIK-related spinal cord K^+ channel (TRESK) and tandem pore domain halothane-inhibited K^+ channel 1 (THIK-1) (Figure 1I and Figure S2). Together, these results suggest that C3001a is a selective TREK-1/2 activator against other K2P channels.

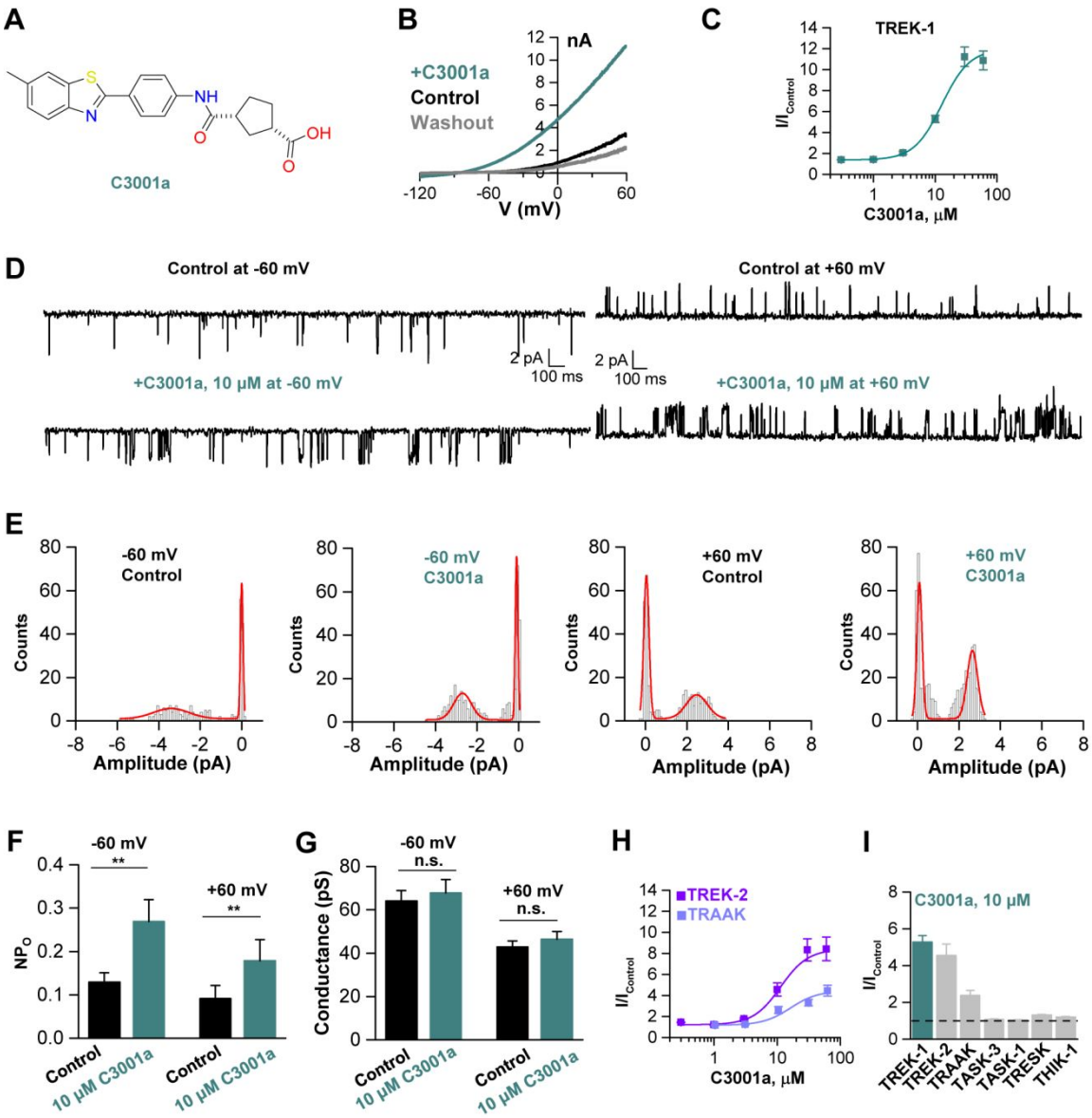

Figure 1. Identification of a TREK-1/2 activator, C3001a. (A) Chemical structure of C3001a. (B) Example whole-cell path-clamp recording of C3001a on TREK-1 channel. (C) C3001a concentration-response curve for TREK-1 with EC_{50} = 12.81 μM (n = 6-23). (D) Representative single-channel current traces from outside-out patches. (E) Amplitude

histograms for the patch recording shown in (D) which were fitted by Gaussian distributions. (F, G) Analysis of NPo (channel number times open probability, F) and channel conductance changes (G) for the single-channel recordings (n = 7; paired *t* test). (H) C3001a concentration-response curves for TREK-2 and TRAAK (n = 6-13) with EC_{50} = 11.31 μM, and 15.29 μM, respectively. (I) Summary for the effects of C3001a (10 μM) on several K2P channels (n = 5-12). Data are shown as means ± SEM. ** $P < 0.01$, n.s., not significant.

Binding mode of C3001a to TREK-1. To determine the binding modes of C3001a to TREK subfamily members, we first analyzed pockets in reported crystal structures of TREK subfamily members by using Fpocket 2.0 server[30]. In this computation, a druggability score greater than 0.5 (the threshold) means that the pocket might be druggable[30]. 32 pockets with druggability scores greater than 0.5 were identified (Figure S3). Then we docked C3001a into each of the pockets by using Glide. The docking results suggested that C3001a may bind to the extracellular crevice formed by P1 and TM4. The

docking scores (Gscores) of C3001a to this crevice in many structures are the top ones (Figure S3). Since the docking score of C3001a to the P1-M4 pocket (the cryptic binding site) in the reported TREK-1 structure with Protein Data Bank (PDB) code of 6CQ8 is the best compared to other reported K2P structures, this crystal structure was adopted for further computational study. And hereafter the P1-M4 pocket was described as the cryptic binding site named by Lolicato et al.[23]. Of note, identification of the extracellular cryptic binding site as potential binding site of C3001a is consistent with the results of inside-out and outside-out patches, which suggests that C3001a binds to the extracellular side of TREK-1.

Next, given the protein flexibility and environmental effects, RosettaLigand was applied to further characterize the binding modes of C3001a to the cryptic binding site. Six starting points were applied for the ligand centroid to scan every site in the pocket as far as possible. 1000 docking poses with lowest total energy score were selected and clustered into eight possible binding models, whose scores are shown in Figure S4A. We selected and analyzed the three top-ranked binding models (Model 1-3), and found that the

carboxyl group of C3001a forms a hydrogen bond with Y285 in Model 2, whereas it interacts with K286 in Model 1 and Model 3 (Figure S4A). To determine which computational model is the correct one, we carried out mutagenesis studies where mutation Y285A significantly reduced the activation efficacy of C3001a on TREK-1 (current enhancement of ~2-fold at 10 μM), whereas mutation K286A did not have marked effect in the activation efficacy (current enhancement of ~4.9-fold at 10 μM, Figure 2A and Figure S4B). Therefore, the mutagenesis data are so far consistent with the interactions between Y285 and the carboxyl group of C3001a predicted in Model 2, rather than Model 1 or Model 3. Next, we designed two derivatives in which the carboxyl group was substituted with hydrogen or methoxycarbonyl group to disturb the hydrogen bond interaction of C3001a with Y285 (Scheme 1 and 2). The two derivatives (30 μM) showed little activation effects on TREK-1, supporting that the carboxyl group of C3001a is essential for activity (Figure 2B,C).

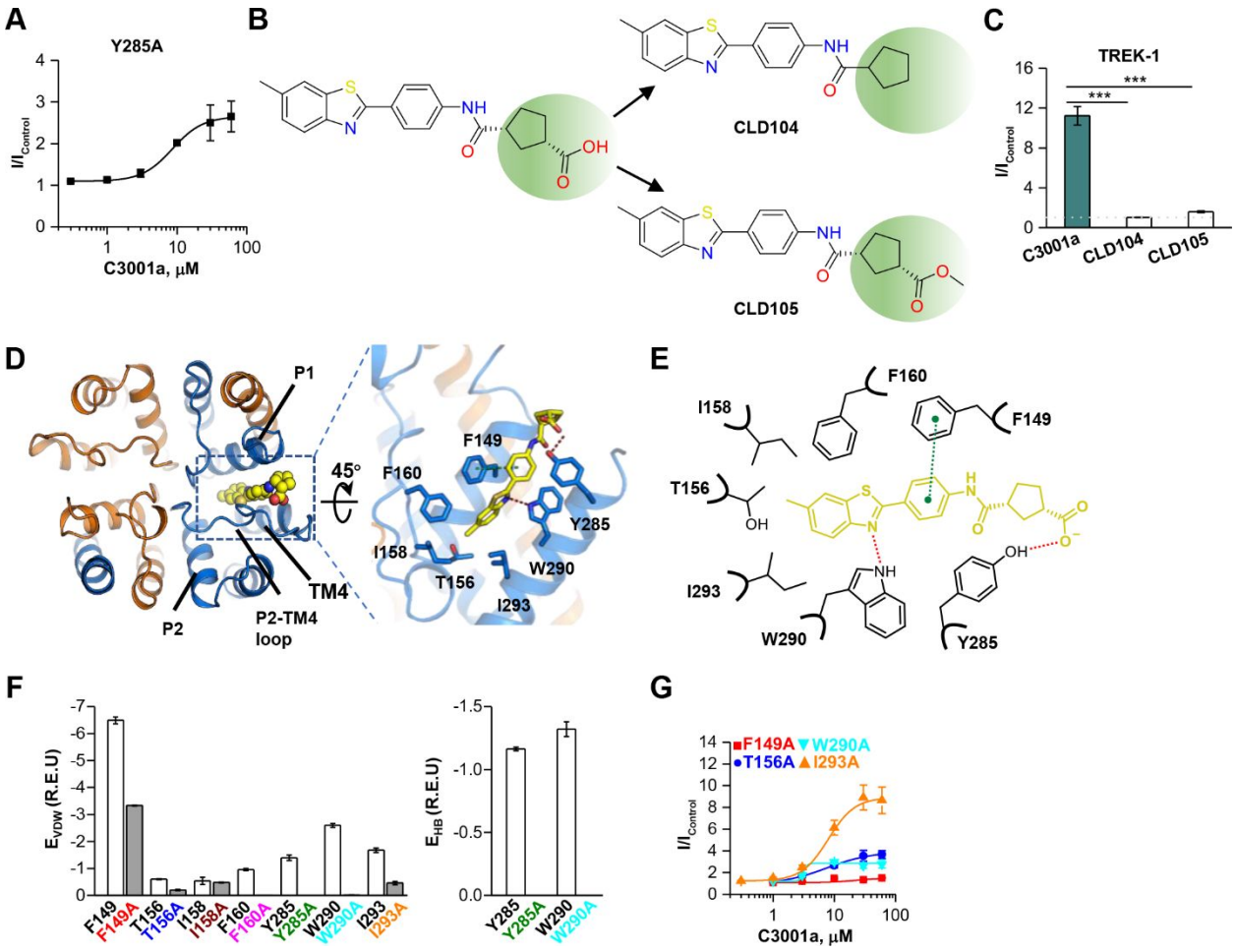

Figure 2. Binding mode of C3001a in TREK-1. (A) Concentration-response curve for C3001a on mutation Y285A with EC50 = 7.86 μM (n = 5-10). (B, C) Chemical structures and effects of two C3001a derivatives: CLD104 and CLD105 (30 μM) on TREK-1 WT (n = 5-6, one-way ANOVA with Dunnett's post hoc test). (D) The top view and detailed view of the predicted binding mode. The TREK-1 structure with PDB code of 6CQ8 was used for building this model. (E) 2D diagram shows interactions between C3001a and TREK-1. (F) Computations show the contributions of seven residues and their mutations to C3001a binding (n = 10, top 10 docking models). E_{VDW} and E_{HB} represent energy

distributions of VDW and hydrogen bond interactions, respectively. Energy unit is Rosetta Energy Unit (R.E.U.). (G) Concentration-response curves for C3001a on four mutations (F149A, T156A, W290A and I293A), yielding EC50 of 22.43 μM, 7.57 μM, 3.91 μM and 7.98 μM, respectively (n = 6-13) Data are shown as means ± SEM. ***P < 0.001.

Scheme 1. Synthesis of CLD104[a].

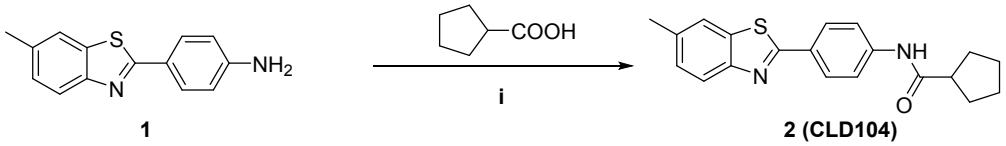

[a]Reagents and conditions: (i) HATU, DIPEA, DCM, rt, 12 h; (CLD104 yield: 83%).

Scheme 2. Synthesis of CLD105 and C3001a[a].

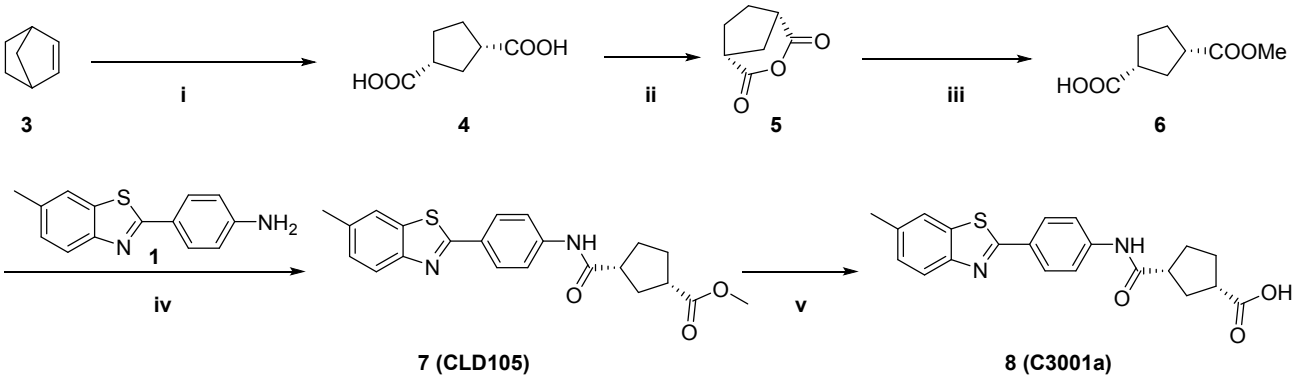

[a]Reagents and conditions: (i) $RuCl_3$, $NaIO_4$, EtOAc, MeCN, water, rt, 12 h; (ii) Ac_2O, 150 °C, 30 min; (iii) MeOH, 80 °C, 5 h; (iv) HATU, DIPEA, DCM, rt, 12 h; (v) LiOH, THF, water, rt, 8 h; (CLD105 yield: 82%; C3001a yield: 63%).

The detailed information of Model 2 is shown in Figure 2D. In this model, in addition to Y285, residues F149, T156, I158, F160, W290, and I293 are close to C3001a and may provide hydrophobic interactions with the benzothiazole or benzene ring of C3001a. Also, W290 may establish a hydrogen bond with benzothiazole nitrogen of C3001a (Figure 2D,E). To further verify the binding mode, we calculated the influence of mutations F149A, T156A, I158A, F160A, Y285A, W290A and I293A on the binding of C3001a by comparing binding contributions of each single residue and that of their mutants (Figure 2F). The computation of energy distributions of the average van der Waals (VDW) interactions predicted that compared with wild type (WT) TREK-1, F149A, T156A, F160A, Y285A, W290A and I293A should reduce the binding of C3001a whereas I158A may not have significant effects (Figure 2F, Left). Moreover, in Y285A and W290A, the contributions of

hydrogen bond energy of Y285 and W290 to ligand binding were significantly reduced (Figure 2F, Right). Then we carried out electrophysiological experiments to test the effects of these mutations on the C3001a activation of TREK-1. I158A and F160A mutations led to nonfunctional channels (Figure S4C). For other functional mutants, expect for I293A, F149A, T156A, Y285A and W290A displayed markedly reduced responses to C3001a (Figure 2A,G). So far, by combining computation with functional mutagenesis, we provide a few structural determinants for the binding of C3001a in the cryptic binding site (Figure 2D,E).

G275 is a residue located at the mouth of the ligand binding pocket (Figure 3A). Although G275 does not form direct interaction with C3001a, introducing a side chain at this position should reduce the entrance size of the pocket and as a result may impede the binding of C3001a to the pocket (Figure 3A). We made the cysteine mutant G275C and we found that G275C showed reduced activation by C3001a (Figure 3B,C). Introducing a side chain by MTSET to G275C may further seal up the entrance of the pocket. Indeed, application of MTSET reduced the activation of C3001a on G275C.

MTSET did not show any significant effect on the TREK-1 WT channel (Figure 3C), whereas MTSET further right-shifted the concentration-response curve for C3001a on G275C (Figure 3D). These results further support that C3001a binds to the cryptic binding site.

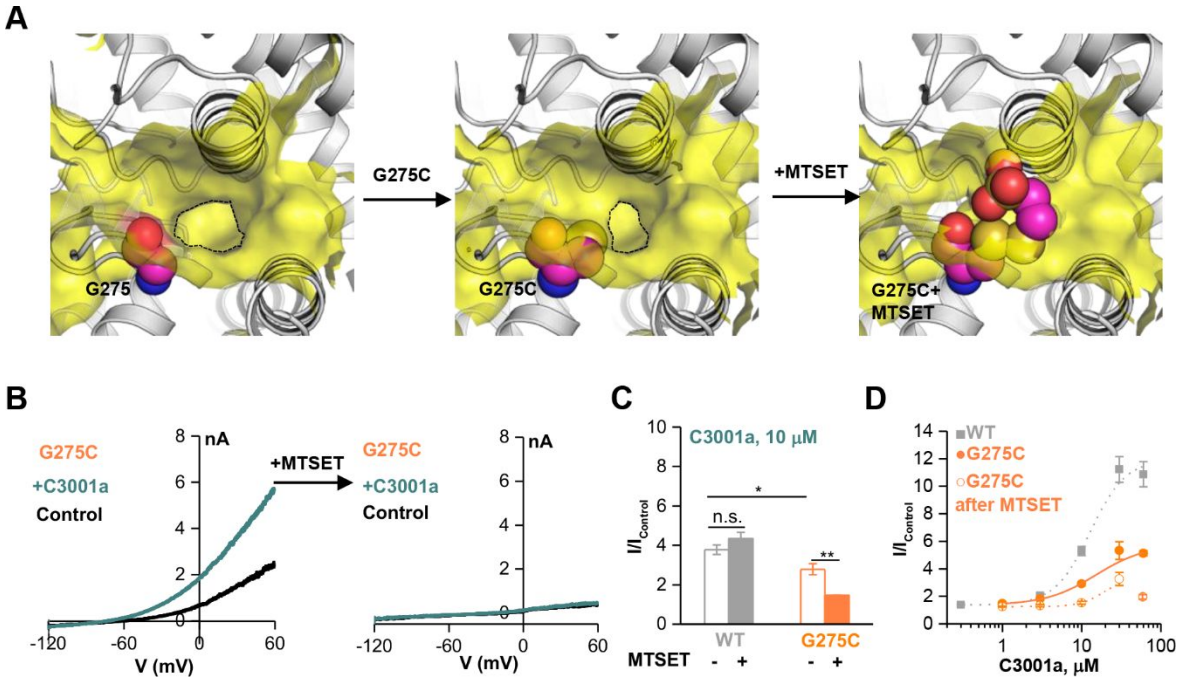

Figure 3. C3001a activity on G275C. (A) Pocket changes by G275C mutation or G275C modified with MTSET (PDB code: 6CQ8). (B) Example whole-cell path-clamp recordings of C3001a on G275C mutation before (*Left*) and after (*Right*) MTSET (1 mM). (C) Summary for the effects of C3001a (10 μM) on TREK-1 WT and G275C without (or with)

MTSET (1 mM) (n = 4-5 cells, one-way ANOVA with Tukey's post hoc test). (D) Concentration-response curves of G275C mutation and G275C modified with MTSET on C3001a activity with EC_{50} = 15.19 μM and 18.40 μM, respectively (n = 5-19). Data are shown as means ± SEM. *P < 0.05, **P < 0.01, n.s., not significant.

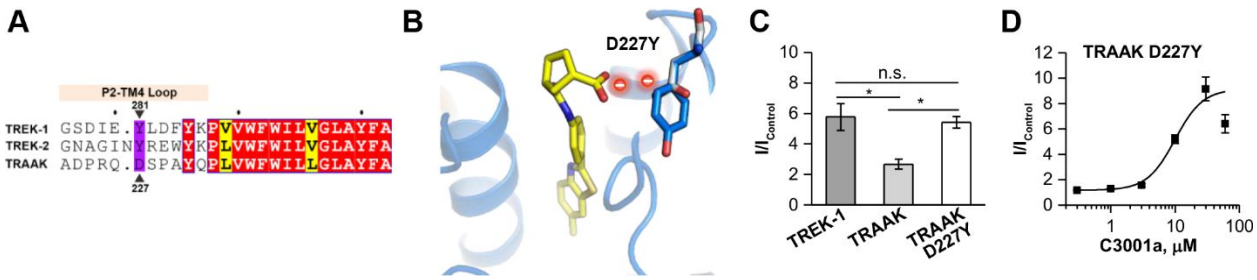

Figure 4. D227 contributes to C3001a selectivity between TREK-1/2 and TRAAK. (A) Sequence alignment of TREK subfamily. (B) Structure presentation of D227Y mutation in the proposed binding model (Models were built based on the TREK-1 structure with the PDB code of 6CQ8). (C, D) The effects of C3001a (10 μM) (C) and the concentration-response curve of C3001a (D) on TRAAK mutation D227Y with EC_{50} = 9.96 μM (n = 4-10, one-way ANOVA with Tukey's post hoc test in (C)). Data are shown as means ± SEM. *P < 0.05, **P < 0.01, n.s., not significant.

Key determinant for C3001a selectivity on TREK subfamily. Compared with TREK-1 and TREK-2, TRAAK was less sensitive to C3001a. According to the multiple sequence alignment in TREK channels, among the residues near the pocket, the residue Y281 in TREK-1 was conserved in TREK-2, but not in TRAAK (equivalent residue D227, Figure 4A). We tested whether D227 controls the subtype selectivity. TRAAK was modeled based on C3001a/TREK-1 binding model. Apparently, in C3001a/TRAAK complex, the carboxyl group of C3001a forms strong negative electrostatic repulsion with D227 (Figure 4B). Hence, we tested the effect of C3001a on the mutant TRAAK D227Y. As a result, D227Y showed significantly increased activation efficacy (current enhancement of ~5.4-fold at 10 μM) by C3001a, compared with TRAAK WT (current enhancement of ~2.5-fold at 10 μM). This was comparable with that in TREK-1 WT (current enhancement of ~5.7-fold at 10 μM) by C3001a (P = 0.90, Figure 4C, D), demonstrating that the residue D227 in TRAAK is an essential structural determinant for the selectivity of C3001a against TRAAK.

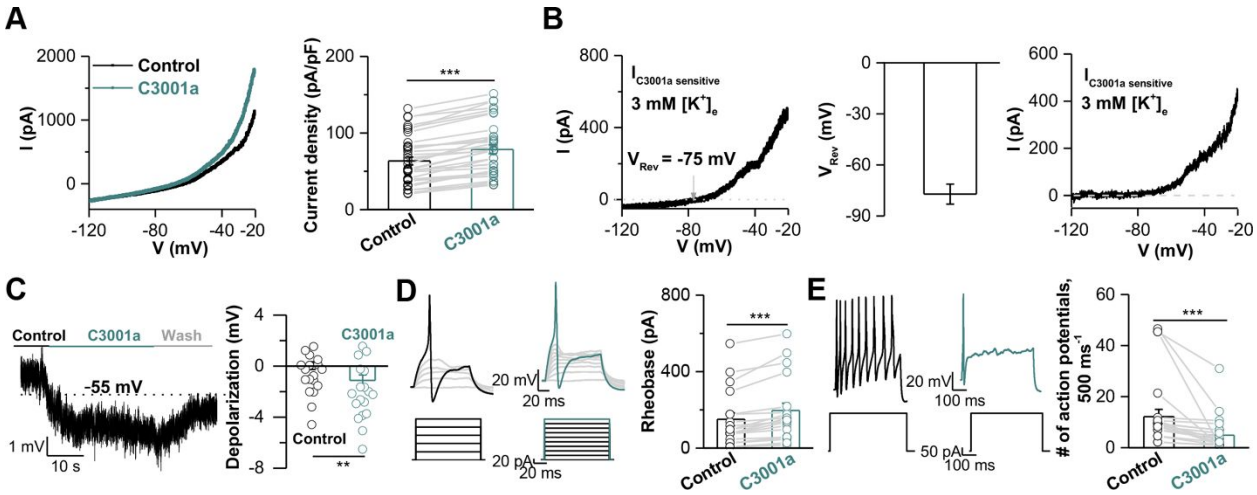

Figure 5. Effects of C3001a on nociceptive neurons. (A) *Left*, representative electrophysiological traces show the effects of C3001a (10 μM) on K^+ currents in DRG neurons; *Right*, bar graph summary for experiments in (*Left*) (n = 35 cells in 4 rats; Wilcoxon signed rank test). (B) *Left*, representative trace shows C3001a-sensitive currents at extracellular 3 mM K^+ concentrations with reversal potential at -75 mV; *Middle,* bar graph shows the average reversal potential around -77 mV in (*Left*) (n = 4 cells of 35 cells in *A*); *Right*, representative trace shows C3001a-sensitive currents at extracellular 3 mM K^+ concentrations without determined reversal potential. (C) Representative trace and bar graph show the effects of C3001a on RMP changes (n = 18 cells in 4 rats; paired *t* test). (D, E) Traces and bar graph show the effects of C3001a on rheobase and firing

frequency in nociceptive neurons (n = 19 cells in 4 rats; Wilcoxon signed rank test in (D) and (E)). Data are shown as means ± SEM. $^{**}P < 0.01$, $^{***}P < 0.001$.

Functional effects of C3001a on dorsal root ganglion (DRG) neurons. The functional effects of C3001a on TREK channels were further examined in dissociated DRG neurons. Recordings were focused on small-sized DRG neurons (diameter of ~20 μm, cell capacitance of ~20 pF), in which the TREK channels were functionally identified[14]. To minimize activation of voltage-gated K^+ current, we applied voltage ramps from -20 mV to -120 mV. In 55 cells recorded, 35 cells responded to C3001a (C3001a-sensitive cells). In the C3001a-sensitive cells, C3001a enhanced the whole-cell current density (in pA/pF) by about 24% (Figure 5A). We subtracted the C3001a-sensitive current, and found that this current was strongly outwardly rectifying (Figure 5B). Only in 4 cells, the reversal potential could be reliably determined, which was around -77 mV, a value that was close to the reversal potential of K^+. In the other 31 cells, the fraction of C3001a-sensitive current was negligible between -120 mV and -60 mV (Figure 5B), making the reversal

potential of the C3001a-sensitive current difficult to resolve. In addition, the application of C3001a resulted in a slight hyperpolarization of the RMP by 1.12 ± 0.42 mV (Figure 5C).

Furthermore, we explored how C3001a regulated the excitability of DRG neurons. In 19 out of 48 neurons, C3001a increased the rheobase (the minimum current required to elicit the first action potential) by ~30% and decreased the number of action potentials evoked by suprathreshold current injections by ~60% (Figure 5D,E). In the other 29 cells, C3001a did not modify the rheobase and slightly increased the frequency of action potentials by 6% (Figure S5). Collectively, our electrophysiological data suggest that C3001a increases the K^+ conductance, hyperpolarizes the RMP, and reduces the excitability in a subset of nociceptive DRG neurons.

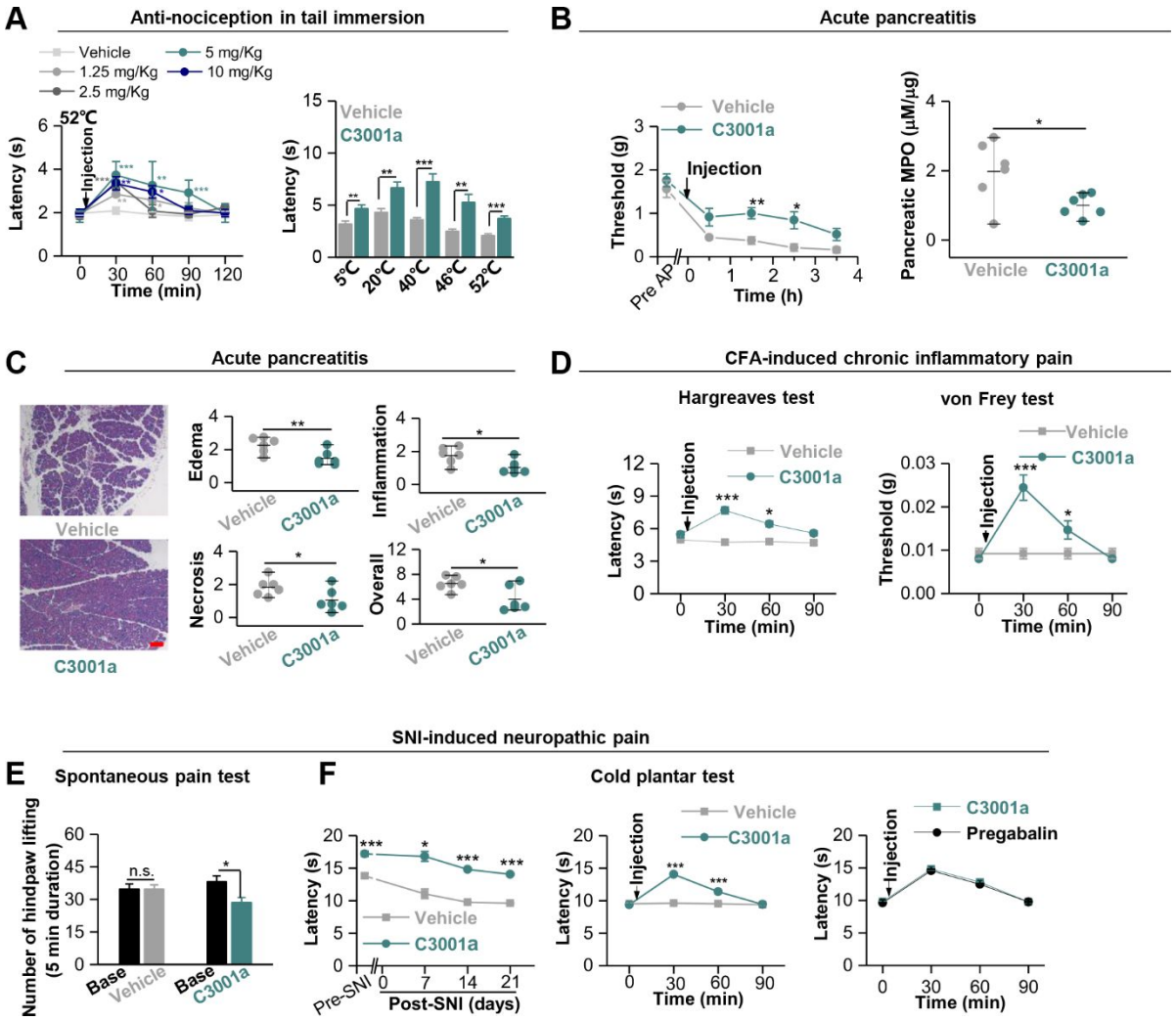

Figure 6. Analgesic and anti-inflammatory effects of C3001a in rodents. (A) *Left*, time course of dose-dependent analgesia by C3001a (1.25, 2.5, 5, 10 mg/kg i.p.) in tail immersion test at 52 °C (n = 6-9; unpaired *t* test or Mann-Whitney test); *Right*, the analgesic effect of C3001a (5 mg/kg i.p.) in tail immersion tests at different temperatures (n = 9-17; unpaired *t* test or Mann-Whitney test); (B) *Left*, time course of the effect of

C3001a (10 mg/kg i.p.) on mechanical allodynia in AP mice (n = 5-6, unpaired *t* test); *Right,* scatter plots show the effect of C3001a on MPO activity in AP mice (n = 6, unpaired *t* test); (C) Representative images and scatter plots show the effect of C3001a (10 mg/kg i.p.) on pancreatic histopathological changes and scores including edema, inflammation and necrosis in AP mice (n = 6, unpaired *t* test or Mann-Whitney test. Scale bar: 100 μm). (D) Summary of C3001a (5 mg/kg i.p.) analgesia in CFA-induced chronic inflammatory pain. *Left*, time course of the effects of C3001a on heat hyperalgesia (n = 9-10; unpaired *t* test); *Right*, time course of the effects of C3001a on mechanical allodynia (n = 9-10; Wilcoxon signed rank test). (E) Effects of C3001a (5 mg/kg i.p.) on spontaneous pain within a 5 min duration on the day 7 after SNI (measured at 30 min post injection, n = 7; unpaired *t* test). (F) *Left*, summary for the effect of C3001a (5 mg/kg i.p.) on cold hyperalgesia at different stages in SNI (n = 8-10; unpaired *t* test or Mann-Whitney test); *Middle*, time course of the effects of C3001a on cold hyperalgesia in SNI mice (n= 8; unpaired *t* test); *Right*, comparison of the effects of C3001a and pregabalin (30 mg/kg, i.p.) on cold plantar test in SNI mice (n = 9; unpaired *t* test); Data are shown as means ± SEM. *$P < 0.05$, **$P < 0.01$, ***$P < 0.001$, n.s., not significant.

Analgesic and anti-inflammatory effects of C3001a in rodents. The TREK activators reported by Vivier et al[26], showed in vivo anti-nociceptive activity. However, the expression of TREK members was downregulated in chronic pain[15, 27, 28] and whether the activation of TREK-1/2 under chronic pain is analgesic remains to be determined. The pharmacokinetic profile of C3001a (Table S1) showed a negligible brain concentration of C3001a and a relatively high concentration of C3001a in the plasma, which suggests that C3001a may exert analgesic functions through TREK family expressed in the peripheral nervous system (PNS). We systematically evaluated the effects of C3001a in analgesia. The anti-nociceptive effect of C3001a was first assessed in the tail immersion test at 52 °C in mice. C3001a displayed dose-dependent analgesia, with a maximal effect at a dose of 5 mg/kg reached 30 min after intraperitoneal (i.p.) injection (Figure 6A, *Left*). C3001a was effective in response to noxious cold (5 °C) or heat stimuli (46 °C and 52 °C) and to physiological stimuli (20 °C and 40 °C) (Figure 6A, *Right*). To further confirm that C3001a was targeting TREK family to be analgesic, CLD104, the derivative of C3001a with no

activity on TREK-1 up to 30 μM (Figure 2B), was used as a negative control. CLD104 showed no analgesic function in tail immersion test (Figure S6A). AP represents a clinically relevant visceral pain model with strong neurogenic inflammation, which could be inhibited by TRPV1 and transient receptor potential ankyrin 1 (TRPA1) antagonists[31, 32]. Recent study suggested that morphine, widely used for the management of pain in AP, may worsen its severity in AP[2]. Furthermore, there are few effective analgesics without side effects or with beneficial influences on anti-inflammatory effects in AP in current clinical managements[33, 34]. Thus, we assessed the analgesic effects of C3001a in a mouse model of cerulein-induced AP[35]. In this model, mechanical allodynia, increased myeloperoxidase (MPO) activity, and significant morphological damage in the form of necrosis, inflammatory infiltration and pancreatic edema were observed (Figure S6B,C). Administration of C3001a (10 mg/kg, i.p.) significantly alleviated mechanical allodynia, reduced MPO activity, and attenuated pancreatic necrosis, inflammation and edema (Figure 6B,C). We detected robust neuronal expression of TREK-1 and TREK-2 mRNA by in situ hybridization using RNAscope in DRG in naïve mice, which were both downregulated in cerulein treated mice (Figure S6D). In contrast, no pancreatic

expression of TREK-1 and TREK-2 mRNA was detected in the pancreas in naïve or cerulein treated mice (Figure S6E), suggesting a neurogenic role of TREK channels in the pathogenesis of analgesia and anti-inflammation in AP. Additionally, the negative control compound CLD104 was ineffective in attenuating pancreatic MPO activity or morphological damage of pancreas in cerulein treated mice (Figure S6F,G). In a mouse model of chronic inflammatory pain developed by intraplantar injection with the complete Freund's adjuvant (CFA), C3001a alleviated heat hyperalgesia and mechanical allodynia (Figure 6D). In the spared nerve injury (SNI)-induced neuropathic pain mouse model, the number of hindpaw lifting, a robust behavior associated with spontaneous pain, was reduced following C3001a administration on day 7 after SNI (Figure 6E). In the cold plantar test, during SNI development (SNI 7 days) and maintenance (SNI 14 days and 21 days), C3001a attenuated cold hyperalgesia with similar potency compared to pregabalin (Figure 6F). In summary, our data suggests that C3001a is effective in treating thermal hyperalgesia and mechanical allodynia in mouse models for acute or chronic pathological pain and pain-associated neurogenic inflammation.

DISCUSSION

For the discovery and modification of small molecule modulators, understanding the molecular recognition basis between the small molecules and the targeted proteins is critical. The currently available crystal structures of TREK channels provide a platform for revealing the binding site of small molecules by using computations. We analyzed potential druggable pockets across TREK subfamily crystal structures followed by molecular docking to identify the possible binding sites of C3001a. By solving the complex crystal structures of TREK-1 with ML335 and its derivatives, Lolicato et al. revealed a cryptic selectivity filter binding site for TREK-1 activators[23]. We compared the binding modes of ML335 and its derivatives in crystal structures with that of C3001a. We found that C3001a forms hydrophobic interactions with F149 and W290 which were similar to the interactions between the equivalent residues F134 and W275 with ML335 and its derivatives in crystal structures. However, C3001a forms a hydrogen bond interaction with Y285 (Y270 in the crystal structures) through its carboxyl group whereas the sulfonyl group of ML335 or its derivatives forms interactions with H141 and S146 (equivalent to

H126 and S131 in the crystal structures). These differences are likely due to the flexibility of both the extracellular loops and the polar groups of the compounds. The identified binding pocket of C3001a was partially overlapped with that of ML335, which further supports that this region is a ligand binding site which could accommodate different chemotypes[23]. The C3001a binding site was confirmed using several approaches. First, the inside-out and outside-out patch experiments indicated that C3001a binds to the extracellular side of the channel. Second, the contributions of several key residues that line the binding site were calculated by RosettaLigand and validated by functional mutagenesis test. Third, we synthesized two C3001a analogues to further confirm the critical role of the carboxyl group of C3001a in TREK-1 binding. Last, the accessibility of C3001a to the binding pocket was examined by a real time covalent modification of the cysteine mutant of a residue located at the entrance of the pocket. Thus, with computation, mutagenesis and chemistry, we provide the binding mechanisms of C3001a to TREK-1. Of note, because the carboxyl group faces to the solvent, we cannot rule out the possibility that the carboxyl group may be structurally flexible. Future structural biology work may be needed to further elucidate the binding of C3001a to TREK channels. Furthermore, the

negatively charged group may also contribute to the weak permeability of C3001a to the blood brain barrier[36]. The utility of the carboxyl group should be further explored as far as the development of C3001a-based next generation selective activators/inhibitors targeting TREK channels in PNS or central nervous system (CNS) is concerned. Our study identified the residue D227 in TRAAK as a key determinant for the subtype selectivity of C3001a. The D227Y mutation showed markedly increased C3001a-mediated activation as compared to the TREK-1 WT. Further studies on the structure-function relationship on TRAAK/C3001a may help identify selective TRAAK inhibitors or activators, which may be served to treat cerebral ischemia[37] or pain.

The pharmacokinetic profiles of the previously identified selective activators including BL-1249, ML67-33, ML335, ML402, and GI-530159 are unclear[21-24]. Our pharmacokinetic analysis show that C3001a acts predominantly on TREK channels in PNS rather than those in the CNS, which allowed us to directly evaluate the analgesic potential of activating TREK channels expressed in PNS. Our in vivo data provide direct evidence to support that activation of TREK channels in PNS is effective in treating polymodal

pathological pain in rodents including thermal hyperalgesia and mechanical allodynia. We consider C3001a analgesia on TREK channels in PNS but not those in CNS as an advantage, since peripheral targets usually have lower risks in drug dependence/addiction[38].

Stimulation of peripheral sensory nerve terminals produces Ca^{2+}-mediated vesicular release of neuropeptides like SP and calcitonin gene related peptide, to generate neurogenic inflammation characterized by increased vascular permeability and vasodilatation. It has been shown that ablating $Nav1.8^{+}$ sensory neurons or silencing them with local anesthetics could reduce allergic airway inflammation[39]. In AP, blocking TRPV1 and TRPA1 activity was shown to be effective in attenuating pain and pancreatic inflammation in cerulein-induced AP[32]. There is increasing pre-clinical and clinical evidence to support that thoracic epidural analgesia may be used as an effective way to treat AP[40, 41]. In accord, we show that TREK-1/2 channels in sensory neurons were downregulated in AP, and enhancing TREK channel activity reduced pain and pain associated neurogenic inflammation. In light of this, we propose that the therapeutic

potential of activating TREK channels should be further explored in other models of AP as well as in other diseases associated with pain and neurogenic inflammation.

In summary, using electrophysiology, computational modeling, we discovered a selective TREK activator C3001a, and provided molecular recognition basis of C3001a in a predicted binding site within TREK-1, which allows to gain insights into channel activation and sub-type selectivity and rationalize subsequent optimization. Using C3001a and in vivo pharmacology, our study establishes the TREK channels in PNS as a therapeutic target in analgesia and pain associated neurogenic inflammation that may be devoid of opioid-like adverse effects.

EXPERIMENTAL SECTION

Material and Instrumentation. All reagents and solvents were commercially purchased from Alfa Aesar, Adamas, or Shanghai Titan Ltd. (Shanghai, China), and used without further purification. HPLC analysis was performed on a Shimadzu LC-10AT HPLC system with a C-18 column (5 μm, 4.6 × 150 mm) at 25 °C. HPLC analysis showed that the purity of all the final products were more than 95%. ^{1}H NMR spectra were recorded on 400 or 600 MHz (100 or

150 MHz for ^{13}C NMR) agilent NMR spectrometer with $CDCl_3$ or DMSO-d_6 as the solvent and tetramethylsilane (TMS) as the internal standard. Chemical shifts were reported in parts per million (ppm, δ scale) downfield from TMS at 0.00 ppm and referenced to the $CDCl_3$ at 7.26 ppm (for ^1H NMR) and 77.16 ppm (for ^{13}C NMR) or the DMSO-d_6 at 2.50 ppm (for ^1H NMR) and 39.52 ppm (for ^{13}C NMR). Liquid chromatography-mass spectrometry (LC-MS) analysis was performed using Agilent LC-MS SQ with electrospray ionization (ESI).

We synthesized (1*S*,3*R*)-3-((4-(6-methylbenzo[*d*]thiazol-2-yl)phenyl)carbamoyl)cyclopentane-1-carboxylic acid (C3001a) and its two analogues (CLD104 and CLD105) (Scheme 1 and 2).

General Procedures for Synthesis of *N-(4-(6-methylbenzo[d]thiazol-2-yl) phenyl) cyclopentanecarboxamide* (CLD104). To a mixture of cyclopentanecarboxylic acid (137 mg, 1.2 mmol) in DCM (10 ml), DIPEA (258 mg, 2 mmol) and HATU (570 mg, 1.5 mmol) were added at room temperature. After stirring for 15 minutes, 4-(6-methylbenzo[d]thiazol-2-yl) aniline (**1**) (240 mg, 1 mmol) was added and the mixture was stirred for 12 hours at room temperature. The reaction mixture was then extracted with DCM and water. The organic layer was washed with water and dried over anhydrous $MgSO_4$, then the solvent was removed under reduced pressure. The crude was then

purified by flash column chromatography on silica gel using pentane/EtOAc (4:1) to obtain the desired pure product compound **2** (CLD104) as a white solid; Yield 83%. HPLC purity: 99.1%. ^{1}H NMR (400 MHz, $CDCl_3$) δ 8.03 (d, J = 8.1 Hz, 2H), 7.91 (d, J = 8.2 Hz, 1H), 7.72–7.62 (m, 3H), 7.33–7.27 (m, 2H), 2.80–2.61 (m, 1H), 2.49 (s, 3H), 2.03–1.86 (m, 4H), 1.86–1.73 (m, 2H), 1.70–1.60 (m, 2H). ^{13}C NMR (150 MHz, $CDCl_3$, Overlapping peaks) δ 174.8, 152.4, 140.6, 129.5, 128.4, 128.0, 122.6, 121.5, 119.7, 47.2, 30.7, 26.2, 21.7. LC-MS: m/z = 337.1$[M+H]^+$.

General Procedures for Synthesis of *Methyl(1S,3R)-3-((4-(6-methylbenzo[d]thiazol-2-yl)phenyl)carbamoyl)cyclopentane-1-carboxylate* (CLD105) and *(1S,3R)-3-((4-(6-methylbenzo[d]thiazol-2-yl)phenyl)carbamoyl)cyclopentane-1-carboxylic acid* (C3001a).

To a solution of $RuCl_3$ (46 mg, 2.2 mol %) in EtOAc/MeCN/water (28 ml, v:v:v = 2:2:3), $NaIO_4$ (8.56 g, 40 mmol) was added and the mixture was cooled to 0 °C. Bicyclo[2.2.1]hept-2-ene (**3**) (941 mg, 10 mmol) was then added slowly and the mixture was warmed to room temperature and stirred for 12 hours. The reaction mixture was quenched and extracted with EtOAc and water. The aqueous layer was extracted by

EtOAc and the organic layers was dried and concentrated under vacuum to obtain the desired product compound **4**. Compound **4** was used for the subsequent dehydration without further purification.

The solution of compound **4** in acetic anhydride (10 ml) was heated at 150 °C by microwave for 30 min, then the solvent was removed under reduced pressure to obtain compound **5**. The product was used for the next step without further purification.

The solution of compound **5** in MeOH (12 ml) was heated and stirred at 80 °C for 5 hours. The solvent was removed under reduced pressure and the residue was purified with flash column chromatography on silica gel by using DCM/MeOH (50:1) mixture as eluent to obtain the desired product compound **6** as colorless liquid (1.12 g, 65% yield from compound **3**).

Compound **7** (CLD105) was synthesized by compound **6** using the same procedure as compound **2**. Compound **7** was obtained as a white solid; Yield 82%. HPLC purity: 99.6%. ^{1}H NMR (400 MHz, $CDCl_3$) δ 8.68 (s, 1H), 8.02 (d, *J* = 7.4 Hz, 2H), 7.91 (d, *J* = 8.1 Hz, 1H), 7.74 (d, *J* = 7.6 Hz, 2H), 7.67 (s, 1H), 7.31–7.26 (m, 1H), 3.76 (s, 3H), 3.04–2.84 (m, 2H), 2.49 (s, 3H), 2.32–2.19 (m, 2H), 2.16–1.91 (m, 4H). ^{13}C NMR (150 MHz, $CDCl_3$) δ

177.8, 174.2, 166.7, 152.5, 152.4, 141.0, 135.3, 129.3, 128.3, 128.0, 122.6, 121.5, 119.7, 52.4, 47.6, 44.1, 32.9, 31.0, 31.0, 21.7. LC-MS: m/z = 395.1$[M+H]^+$.

To a solution of compound **7** (197 mg, 0.5 mmol) in THF/water (10 ml, v:v = 4:1), LiOH(48 mg, 2 mmol) was added at room temperature. After stirring for 8 hours, the reaction mixture was diluted with EtOAc and water. The aqueous layer was washed with EtOAc for two more times. Diluted hydrochloric acid was added to the aqueous layer until the pH value reached 2, then the precipitated crystal was filtered. The crystal was washed with water and dried under reduced pressure. 120 mg Compound **8** (C3001a) was obtained.; Yield 63%. HPLC purity: 98.8%. ^{1}H NMR (400 MHz, DMSO-d_6) δ 12.14 (s, 1H), 10.24 (s, 1H), 8.00 (d, J = 8.5 Hz, 2H), 7.92–7.83 (m, 2H), 7.80 (d, J = 8.5 Hz, 2H), 7.33 (d, J = 8.4 Hz, 1H), 2.95–2.82 (m, 1H), 2.83–2.69 (m, 1H), 2.44 (s, 3H), 2.25–2.10 (m, 1H), 2.05–1.71 (m, 5H). ^{13}C NMR (100 MHz, DMSO-d_6) δ 177.4, 174.6, 166.8, 152.7, 143.0, 135.9, 135.4, 128.9, 128.7, 128.5, 123.1, 122.7, 120.3, 46.5, 44.4, 34.4, 30.5, 29.9, 22.0. LC-MS: m/z = 381.1$[M+H]^+$.

Molecular biology. The cDNAs of TREK-1 (human, NM_001017425.3), TREK-2 (mouse, NM_029911.5) and TRAAK (human, NM_033310.2) were subcloned into the pEGFPN1

expression vector (Invitrogen, US). The cDNAs of TASK-3 (human, NM_001282534.2), TASK-1 (human, NM_002246.3), THIK-1 (human, NM_022054.4) and TRESK (human, NM_181840.1) were subcloned into the pCDNA3 vector (Invitrogen, US). Electrophysiology tests of TREK-1, TREK-2, TRAAK, THIK-1, TRESK, TASK-3, TASK-1, were performed with transiently transfected HEK-293T cells using PolyJet™ reagent. All site-directed mutagenesis were conducted and sequencing confirmed by providers (GENEWIZ, Suzhou, China).

Molecular docking. The crystal structure of TREK-1 (PDB codes 4TWK, 6CQ6, 6CQ8 and 6CQ9), TREK-2 (PDB codes 4BW5, 4XDJ, 4XDK and 4XDL) and TRAAK (PDB code 3UM7, 4I9W, 4RUE and 4RUF, 4WFE, 4WFF, 4WFG, 4WFH)[23, 42-46] were used to detect druggable pockets by using Fpockets 2.0 server[30]. Druggability score was calculated to assess the possibility of a pocket to accommodate drug-like molecules. The score more than 0.5 (the threshold) means the pocket might be druggable. C3001a was docked to each druggable pocket in all structures by using Schrödinger Glide software SP mode. The protonation state of C3001a was assigned by using Ligprep module at pH 7.0 ± 2.0. Glide G-score was used to rank the result list. Considering the energetic effects of the

solvent environment and the receptor flexibility, RosettaLigand[47, 48] was applied to generate accurate molecular docking models of C3001a to the TREK-1 channel. The docking was processed as described previously[5]. The yielded 1000 docking models were sorted by total score of ligand-protein complex. The select_best_unique_ligand_poses application was adopted to cluster the ligand poses by setting RMSD cutoff of 3 Å.

Missing atoms and loops of crystal structure of TREK-1 (PDB code 6CQ8) were built and refined by Discovery Studio 3.0. Modeller was used to create homology models of wild-type TRAAK and several mutants of TREK-1, including F149A, T156A, I158A, F160A, Y285A, W290A and I293A. *In silico* alanine scan were conducted by individually changing residue to alanine without otherwise changing the conformation of protein or ligands in Rosetta. To explore the distribution of binding interactions between compounds and TREK-1 or TREK-1 mutants, the average energy of the top 10 models with the lowest binding energies (interface score) was calculated. To quantitatively analyze the results, the binding energy was decomposed as mainly VDW and H-Bond energy. Further, these energies were mapped on per residue by Rosetta's residue_energy_breakdown utility.

Chemicals. For electrophysiology, stock solutions of C3001a and its derivatives (10 mM) were prepared in dimethyl sulfoxide (DMSO, Sigma, US) and diluted in the extracellular solution to the final concentration before use. MTSET (BOC Sciences, US) was made as stock solution (0.5 M) in DMSO and stored in aliquots at -20 °C. Aliquots were diluted in external solution to a final concentration of 1 mM within 120 s of being applied to cells. For animal studies, C3001a and its derivatives were dissolved in 5% DMSO, 5% Tween 80 and 90% saline. The solvents were used as vehicle controls.

Electrophysiology. Whole-cell recordings of ion channels were performed with a MultiClamp 700B amplifier (Molecular Devices) at room temperature. The current signals were filtered at 2 kHz and digitized at 10 kHz. The pipettes for whole-cell recordings were pulled from borosilicate glass capillaries by using a Flaming-Brown horizontal puller (Model P1000, Sutter Instruments) and had a resistance of 3-7 MΩ. For recordings of K^+ channels, the standard pipette solution contained (in mM) 140 KCl, 3 $MgCl_2$, 5 EGTA, 0.5 $CaCl_2$, and 10 HEPES (pH 7.4, adjusted with KOH), and the external solution contained (in mM) 145 NaCl, 4 KCl, 2 $CaCl_2$, 1 $MgCl_2$, and 10 HEPES and 10 glucose (pH 7.3, adjusted with NaOH). To measure the current-voltage relationships (I-V curves) of K^+

channels, HEK-293T cells were held at -60 mV with a ramp from -120 mV to +60 mV applied for 500 ms and then the cell was repolarized back to -60 mV.

For single channel recordings of TREK-1 channels, HEK-293T cells were transfected with human TREK-1 in the pEGFP-N1 vector. The pipettes had resistances of 7-15 MΩ. The standard pipette and bath solution contained (in mM): 140 KCl, 10 HEPES and 2 EGTA (pH 7.3, adjusted with KOH). During acquisition the single-channel currents were low-pass filtered at 2 kHz and sampled at 10 kHz. Recordings lasting at least 50 s were subject to further analysis to ensure enough events detected. A threshold at half the open channel current amplitude of the major conductance state was set to detect the single channel events. No junction potential correction was done. All the events in the selected section were detected automatically using Clampfit 10 (Molecular Devices) followed by manual inspection. The amplitude histograms were fitted with Gaussian distributions with a bin width of 0.1 pA. TREK-1 channel activity in an outside-out patch was expressed quantitatively as NP_O (N is the number of channels in the patch, and P_O is the probability of a channel being open). The single channel conductance of TREK-1 channel was

calculated using the ratio of current amplitude of the first open state to voltage at -60 mV or +60 mV.

Acutely dissociated DRG neuron preparation and electrophysiology. Five to six-week-old male Sprague-Dawley rats were euthanized with a lethal dose of pentobarbital intraperitoneally. The DRGs were collected in a 35-mm tissue culture dish. They were digested in 0.3% collagenase (Sigma, US) for 20 min at 37 °C, followed by 1% trypsin (Gibco, US) for another 30 min, and the enzymatic treatment were terminated with fetal bovine serum (Gibco, US). After titurating by pipetting up and down, the DRG neurons were cultured in neurobasal growth medium containing 2% B27 (Gibco, US) supplement for 2-4 h. The bath solution contained (in mM) 140 NaCl, 3 KCl, 1.3 $MgCl_2$, 10 HEPES, 2.4 $CaCl_2$, and 10 glucose (pH 7.3, adjusted with NaOH). The pipette solution contained (in mM) 135 KCl, 10 HEPES, 5 EGTA, 10 NaCl, and 4 Mg-ATP (pH 7.4, adjusted with KOH). Under voltage-clamp recording mode, cells were clamped at -60 mV, and series resistance (<15 MΩ) was compensated by 85%. To minimize voltage-gated K^+ currents, the membrane potential was depolarized from a holding potential of -60 mV to -20 mV for 1 s and subsequently hyperpolarized to -120 mV within 1 s. Under current-clamp

recording mode, cells were held at 0 pA, and the firing threshold was first measured by a series of 100-ms depolarizing current injections in 10-pA incremental steps from 0 pA to elicit the first action potential. To further examine the firing properties of the DRG neurons, a large depolarizing current (500 ms, 2.5-fold action potential threshold) was delivered to elicit the cell generating sufficient firing. Whole-cell recordings were performed with hardware settings similar to those described for electrophysiology in HEK-293T cells.

Animals. All procedures were performed on male BALB/c or C57BL/6 mice and Sprague-Dawley rats in the study. 6-8 weeks aged BALB/c or C57BL/6 mice were used for behavioral tests. 5-6 weeks aged rats were used for DRG neuron electrophysiology. Animals were housed in a temperature-controlled environment on a 12 h light-dark cycle with food and water ad libitum. All experiments with mice and rats were approved by the Animal Research Committee at the West China Hospital of Sichuan University (PROTOCOL No.72018175A) and the Animal Research Committee of East China Normal University (PROTOCOL No. m20190329).

Tail immersion. Mice were acclimated in a holder with its tail protruding and moving freely 15 min for 3 days. The terminal 3 cm of the tail was immersed in water at 5 °C,

20 °C, 40 °C, 46 °C, and 52 °C. The latency (in seconds (s)) of tail flick time was determined by a jerk of the tail. A cut-off time of 15 s was imposed to minimize tissue injury.

Acute pancreatitis mouse model. Acute pancreatitis was induced by 7 intraperitoneal injections of cerulein (Tocris; Minneapolis, MN, US) with 50 μg/kg at hourly interval, while control mice received PBS injections as previously described[49]. Cerulein was dissolved in ice cold PBS. Dissolved C3001a and vehicle were injected at 2, 4, 6, 8, 10 h after the first injection of cerulein. Von Frey test was begun at 0.5 h after the last injection of cerulein. Mice were humanly sacrificed 12 h after the first cerulein/PBS injection. Pancreatic tissue was promptly harvested, then divided for measurement of MPO activity, histopathology, and RNAscope.

Pancreatic MPO activity assay and histopathology scoring were performed as previously described[50]. Specifically, histolopathological assessment of pancreatic damage was performed after H&E staining of fixed pancreatic slices (5 mm thickness), 10 random fields per slide from all animal groups were graded by two independent,

blinded observers according to extent of edema, inflammatory cell infiltration and acinar necrosis.

Chronic inflammatory pain model. Complete Freund's Adjuvant (CFA) (Sigma, US) was injected subcutaneously (20 μl) into the left hindpaw to induce chronic inflammation pain in mice. After injection, the syringe was kept for at least 30 s to avoid overflow.

Hargreaves test. The CFA-induced inflammatory mice were acclimated in Plexiglas chambers with a glass floor for 3 days. A radiant heat source (Ugo-Basile, Italy) was aimed at the plantar surface of the left hindpaw through a glass surface. The stimulus intensity was set to produce an approximate latency of 10 s at baseline, and a cut-off value was set at 20 s to avoid unexpected damage. The withdrawal latency was recorded per mouse with a 5 min inter-stimulation period.

von Frey test. The mice were individually placed in an elevated transparent cage (20 × 20 × 14 cm) with a wire mesh floor (0.5 × 0.5 cm) to acclimate to the environment for 3 days before testing. The mechanical paw withdrawal threshold was assessed using von Frey filaments (Ugo-Basile, Italy) with an ascending order. The tip of the filament was perpendicularly targeted to the region, and sufficient stimulation was maintained for 1 s.

Rapid paw withdrawal or flinching was considered a positive response, and the bending force for which at least 60% of the application elicited a positive response was recorded as the mechanical paw withdrawal threshold.

Spared nerve injury model. Mice were anesthetized with 75 mg/kg pentobarbital intraperitoneally. After shaving and disinfection with povidone iodide and 75% ethanol, a minimal skin incision was made on the lateral left mid-thigh to expose the sciatic nerve and its three terminal branches by separating the muscle layers. The tibial and common peroneal nerves were tightly ligated with 5.0 silk threads, and a 1-2 mm of each nerve distal to the ligation was cut and removed. The sural nerve was restrictively preserved to avoid any harmful injury. The muscle layer and skin were closed after surgery, and the animals were transferred to a warm pad to recover from anesthesia.

Spontaneous pain test. After 3 days of acclimation, the SNI mice were individually placed in an elevated transparent cage (20 × 20 × 14 cm) with a wire mesh floor (0.5 × 0.5 cm). A 5 min duration was videotaped by an action camera (SONY, HDR-AS50) for each mouse, and the number of left hindpaw flinches was calculated by a blind experimenter.

Cold plantar test. Mice were acclimated on the glass plate of 6 mm depth for 3 consecutive days. A 5 ml syringe packed with powdered dry ice was used as the cold probe. The center of the left hindpaw of SNI mice was targeted. The withdrawal latency, defined as any action to move the paw vertically or horizontally away from the glass plate, was measured with a stopwatch. A cutoff time of 30 s was used to avoid potential tissue damage.

Pharmacokinetics study. Pharmacokinetics of C3001a was analyzed in BALB/c mice (n = 6). Plasma and brain concentrations were determined using LC-MS/MS methods after a single intraperitoneal injection dose (i.p. 5 mg/kg) of compound as a clear solution in 5% DMSO + 5% Tween80 + 90% saline at a concentration of 0.5 mg/ml. Blood samples were collected into heparinized test tubes at each time point (0.083 h, 0.25 h, 0.5 h, 1.0 h, 2.0 h, 4.0 h, and 8.0 h) and centrifuged at 2,000 g for 15 minutes to generate plasma samples. Brains were collected after myocardial perfusion with normal saline and homogenated with brain: normal saline (1:2, W/V) to generate brain samples. LC-MS/MS methods to quantify C3001a in plasma and brain samples were developed. Plasma and brain samples were extracted with ACN, mixed and centrifuged. The supernatants were

transferred into injection vials. The samples were analyzed with a Shimadzu HPLC system coupled with a 4000 Qtrap mass spectrometer (AB SCIEX), which was equipped with an Applied Biosystems electrospray ionization (ESI) source and operated with Analyst 1.6.3 (AB SCIEX). The column used was an Agela Venusil XBP C18 50 × 2.1 mm, 5 micron column. The mobile phase consisted of A: 5 mM NH_4OAc with 0.1% formic acid in water, and B: MeOH. Standard curves were prepared by spiking compounds into control plasma and brain and these were used to determine drug concentrations. Pharmacokinetic parameters including area under the curve (AUC), T_{max}, C_{max}, and $T_{1/2}$ were calculated via non-compartmental analysis (NCA) using Phoenix WinNolin version 6.4 with mean concentration at each time point.

RNAscope in situ hybridization. The hybridization assay was performed as described in the previous study[5] . The sequences of the target probes, preamplifier, amplifier and label probes are proprietary and commercially available (Advanced Cell Diagnostics, US). The in situ probes included TREK-1 (*Kcnk2* (Cat#440421)), TREK-2 (*Kcnk10* (Cat#535391)). Fluorescence images were taken using a NIKON A1R$^+$ two-photon confocal scanning microscope and were analyzed using ImageJ software.

ASSOCIATED CONTENT

Support Information

Figure S1. Inside-out recordings of TREK-1 with 10 μM C3001a application.

Figure S2. Representative current traces for several K2P channels in response to 10 μM C3001a.

Figure S3. Pocket analysis of TREK channel crystal structures.

Figure S4. Possible binding models based on RosettaLigand docking and their validation.

Figure S5. No inhibitory effects of C3001a on a portion of DRG neurons.

Figure S6. Data for nociception and AP associated with Figure 6.

Table S1. Pharmacokinetic profile of C3001a in plasma and brain following a single intraperitoneal administration to male mice.

Table S2. List of molecular formula strings

Data S1. The binding model of C3001a/TREK-1 complex based on the TREK-1 structure with PDB code of 6CQ8.

Data S2. Homology model of the TRAAK channel based on the TREK-1 structure with PDB code of 6CQ8.

Data S3. Homology model of C3001a/TRAAK complex based on the TREK-1 structure with PDB code of 6CQ8.

Accession codes

The binding model of C3001a/TREK-1 complex, homology model of the TRAAK channel and homology model of C3001a/TRAAK complex were built on the basis of the TREK-1 crystal structure with PDB code of 6CQ8. Authors will release the atomic coordinates upon article publication.

Corresponding Author Information

*E-mail: hyyang@bio.ecnu.edu.cn.

*E-mail: ruotianjiang@scu.edu.cn.

Author Contribution

#Y.Q., L.H. and J.F. contributed equally. The article was written through contributions of all the authors. All the authors have given approval to the final version of the article.

Notes

H.Y., R.J., and Q.Z. are inventors on patent applications (201811416098.3 and PCT/CN2018119641) submitted by West China Hospital of Sichuan University, East China Normal University, and Shaoxing ZeroIn Biomedicines Co. Ltd. that cover the potential usage of C3001a and its derivatives.

ACKNOWLEDGMENT

We thank Zhenpeng Song (Laboratory of Anesthesia and Critical Care Medicine, West China Hospital, Sichuan University) for the engagement at the early phase of the project. We thank Li Li, Fei Chen and Chunjuan Bao (Laboratory of Pathology, West China Hospital, Sichuan University) for HE staining. We thank Jie Zhang, Zhen Yang and Lin Bai (Histology and Imaging platform, Core Facility of West China Hospital, Sichuan University) for fluorescence imaging. We thank Prof. Haoxing Wu for assistance with

mass spectrometry. Thanks to the Research Core Facility, West China Hospital, Sichuan University for sharing instruments.

Funding: Supported by National-Local Joint Engineering Research Center of Translational Medicine of Anesthesiology of West China Hospital of Sichuan University (No. 2019-180), the "Personalized Medicines-Molecular Signature-based Drug Discovery and Development", Strategic Priority Research Program of the Chinese Academy of Sciences (XDA12040220 to H.Y.), the National Science & Technology Major Project “Key New Drug Creation and Manufacturing Program” of China (2018ZX09711002 to Q.Z. and H.Y.), the "XingFuZhiHua" funding of ECNU (44300-19311-542500/006 to H.Y.), the Fundamental Research Funds for the Central Universities (to H.Y. and 2018SCUH0086 to R.J.), the National Natural Science Foundation of China (31600832 to R.J., 21422208 to H.Y), Thousand Talents Plan in Sichuan Province (to R.J.), 1.3.5 Project for Disciplines of Excellence of West China Hospital of Sichuan University (ZY2016101 to J.L.). We thank the support of ECNU Multifunctional Platform for Innovation (001 and 011). The Natural Science Foundation of the Jiangsu Higher Education Institutions of China (Grant

No. 18KJA350001) and the Priority Academic Program Development of the Jiangsu Higher Education Institutes (PAPD).

ABBREVIATIONS

TREK, TWIK-related K^+ channel; TRAAK, TWIK-related arachidonic acid-stimulated K^+ channel; K2P, two-pore domain K^+ channels; AP, acute pancreatitis; TASK-3, TWIK-related acid-sensitive K^+ 3; TM, transmembrane segment; SP, substance P; $IB4^+$, isolectin 4-positive; TRPV1, transient receptor potential cation channel subfamily V member 1; TRPA1, transient receptor potential ankyrin 1; RMP, resting membrane potential; μOR, μ-opioid receptor; TRESK, TWIK-related spinal cord K^+ channel; THIK-1, tandem pore domain halothane-inhibited K^+ channel 1; VDW, van der Waals; R.E.U., Rosetta Energy Unit; MTSET, N,N,N-trimethyl-2-[(methylsulfonyl)thio]-ethanaminium, monochloride; DRG, dorsal root ganglion; i.p., intraperitoneal; SNI, spared nerve injury; DIPEA, N,N-Diisopropylethylamine; HATU, 1-[Bis(dimethylamino)methylene]-1H-1,2,3-triazolo[4,5-b]pyridinium 3-Oxide Hexafluorophosphate; MPO, myeloperoxidase; CFA, Complete Freund's Adjuvant.

REFERENCES

1. Volkow, N. D.; McLellan, A. T. Opioid abuse in chronic pain--misconceptions and mitigation strategies. *N. Engl. J. Med.* **2016,** 374, 1253-1263.

2. Barlass, U.; Dutta, R.; Cheema, H.; George, J.; Sareen, A.; Dixit, A.; Yuan, Z.; Giri, B.; Meng, J.; Banerjee, S.; Banerjee, S.; Dudeja, V.; Dawra, R. K.; Roy, S.; Saluja, A. K. Morphine worsens the severity and prevents pancreatic regeneration in mouse models of acute pancreatitis. *Gut* **2018,** 67, 600-602.

3. Royal, P.; Andres-Bilbe, A.; Avalos Prado, P.; Verkest, C.; Wdziekonski, B.; Schaub, S.; Baron, A.; Lesage, F.; Gasull, X.; Levitz, J.; Sandoz, G. Migraine-associated TRESK mutations increase neuronal excitability through alternative translation initiation and inhibition of TREK. *Neuron* **2019,** 101, 232-245.e6.

4. Yekkirala, A. S.; Roberson, D. P.; Bean, B. P.; Woolf, C. J. Breaking barriers to novel analgesic drug development. *Nat. Rev. Drug. Discov.* **2017,** 16, 545-564.

5. Liao, P.; Qiu, Y.; Mo, Y.; Fu, J.; Song, Z.; Huang, L.; Bai, S.; Wang, Y.; Zhu, J. J.; Tian, F.; Chen, Z.; Pan, N.; Sun, E. Y.; Yang, L.; Lan, X.; Chen, Y.; Huang, D.; Sun, P.; Zhao, L.; Yang, D.; Lu, W.; Yang, T.; Xiao, J.; Li, W. G.; Gao, Z.; Shen, B.; Zhang, Q.; Liu, J.; Jiang, H.; Jiang, R.; Yang, H. Selective activation of TWIK-related acid-sensitive K^+ 3 subunit-containing channels is analgesic in rodent models. *Sci. Transl. Med.* **2019,** 11, eaaw8434.

6. Gada, K.; Plant, L. D. Two-pore domain potassium channels: emerging targets for novel analgesic drugs: IUPHAR Review 26. *Br. J. Pharmacol.* **2019,** 176, 256-266.

7. Levitz, J.; Royal, P.; Comoglio, Y.; Wdziekonski, B.; Schaub, S.; Clemens, D. M.; Isacoff, E. Y.; Sandoz, G. Heterodimerization within the TREK channel subfamily produces a diverse family of highly regulated potassium channels. *Proc. Natl. Acad. Sci. U. S. A.* **2016,** 113, 4194-4199.

8. Maingret, F.; Patel, A. J.; Lesage, F.; Lazdunski, M.; Honore, E. Mechano- or acid stimulation, two interactive modes of activation of the TREK-1 potassium channel. *J. Biol. Chem.* **1999,** 274, 26691-26696.

9. Patel, A. J.; Honore, E.; Maingret, F.; Lesage, F.; Fink, M.; Duprat, F.; Lazdunski, M. A mammalian two pore domain mechano-gated S-like K+ channel. *Embo J* **1998,** 17, 4283-4290.

10. Bockenhauer, D.; Zilberberg, N.; Goldstein, S. A. KCNK2: reversible conversion of a hippocampal potassium leak into a voltage-dependent channel. *Nat. Neurosci.* **2001,** 4, 486-491.

11. Maingret, F.; Lauritzen, I.; Patel, A. J.; Heurteaux, C.; Reyes, R.; Lesage, F.; Lazdunski, M.; Honore, E. TREK-1 is a heat-activated background K(+) channel. *Embo J* **2000,** 19, 2483-2491.

12. Honore, E.; Maingret, F.; Lazdunski, M.; Patel, A. J. An intracellular proton sensor commands lipid- and mechano-gating of the K(+) channel TREK-1. *Embo J* **2002,** 21, 2968-2976.

13. Sandoz, G.; Douguet, D.; Chatelain, F.; Lazdunski, M.; Lesage, F. Extracellular acidification exerts opposite actions on TREK1 and TREK2 potassium channels via a single conserved histidine residue. *Proc. Natl. Acad. Sci. U. S. A.* **2009,** 106, 14628-14633.

14. Alloui, A.; Zimmermann, K.; Mamet, J.; Duprat, F.; Noel, J.; Chemin, J.; Guy, N.; Blondeau, N.; Voilley, N.; Rubat-Coudert, C.; Borsotto, M.; Romey, G.; Heurteaux, C.; Reeh, P.; Eschalier, A.; Lazdunski, M. TREK-1, a K+ channel involved in polymodal pain perception. *Embo J* **2006,** 25, 2368-2376.

15. Acosta, C.; Djouhri, L.; Watkins, R.; Berry, C.; Bromage, K.; Lawson, S. N. TREK2 expressed selectively in IB4-binding C-fiber nociceptors hyperpolarizes their membrane potentials and limits spontaneous pain. *J. Neurosci.* **2014,** 34, 1494-1509.

16. Du, X.; Hao, H.; Gigout, S.; Huang, D.; Yang, Y.; Li, L.; Wang, C.; Sundt, D.; Jaffe, D. B.; Zhang, H.; Gamper, N. Control of somatic membrane potential in nociceptive neurons and its implications for peripheral nociceptive transmission. *Pain* **2014,** 155, 2306-2322.

17. Kanda, H.; Ling, J.; Tonomura, S.; Noguchi, K.; Matalon, S.; Gu, J. G. TREK-1 and TRAAK are principal K^+ channels at the Nodes of Ranvier for rapid action potential conduction on mammalian myelinated afferent nerves. *Neuron* **2019,** P960-971.

18. Pereira, V.; Busserolles, J.; Christin, M.; Devilliers, M.; Poupon, L.; Legha, W.; Alloui, A.; Aissouni, Y.; Bourinet, E.; Lesage, F.; Eschalier, A.; Lazdunski, M.; Noel, J. Role of the TREK2 potassium channel in cold and warm thermosensation and in pain perception. *Pain* **2014,** 155, 2534-2544.

19. Noel, J.; Zimmermann, K.; Busserolles, J.; Deval, E.; Alloui, A.; Diochot, S.; Guy, N.; Borsotto, M.; Reeh, P.; Eschalier, A.; Lazdunski, M. The mechano-activated K+ channels TRAAK and TREK-1 control both warm and cold perception. *Embo J* **2009,** 28, 1308-1318.

20. Devilliers, M.; Busserolles, J.; Lolignier, S.; Deval, E.; Pereira, V.; Alloui, A.; Christin, M.; Mazet, B.; Delmas, P.; Noel, J.; Lazdunski, M.; Eschalier, A. Activation of TREK-1 by morphine results in analgesia without adverse side effects. *Nat. Commun.* **2013,** 4, 2941.

21. Bagriantsev, S. N.; Ang, K. H.; Gallardo-Godoy, A.; Clark, K. A.; Arkin, M. R.; Renslo, A. R.; Minor, D. L., Jr. A high-throughput functional screen identifies small molecule regulators of temperature- and mechano-sensitive K2P channels. *ACS. Chem. Biol.* **2013,** 8, 1841-1851.

22. Schewe, M.; Sun, H.; Mert, U.; Mackenzie, A.; Pike, A. C. W.; Schulz, F.; Constantin, C.; Vowinkel, K. S.; Conrad, L. J.; Kiper, A. K.; Gonzalez, W.; Musinszki, M.; Tegtmeier, M.; Pryde, D. C.; Belabed, H.; Nazare, M.; de Groot, B. L.; Decher, N.; Fakler, B.; Carpenter, E. P.; Tucker,

S. J.; Baukrowitz, T. A pharmacological master key mechanism that unlocks the selectivity filter gate in K(+) channels. *Science* **2019,** 363, 875-880.

23. Lolicato, M.; Arrigoni, C.; Mori, T.; Sekioka, Y.; Bryant, C.; Clark, K. A.; Minor, D. L., Jr. K2P2.1 (TREK-1)-activator complexes reveal a cryptic selectivity filter binding site. *Nature* **2017,** 547, 364-368.

24. Loucif, A. J. C.; Saintot, P. P.; Liu, J.; Antonio, B. M.; Zellmer, S. G.; Yoger, K.; Veale, E. L.; Wilbrey, A.; Omoto, K.; Cao, L.; Gutteridge, A.; Castle, N. A.; Stevens, E. B.; Mathie, A. GI-530159, a novel, selective, mechanosensitive two-pore-domain potassium (K2P) channel opener, reduces rat dorsal root ganglion neuron excitability. *Br. J. Pharmacol.* **2018,** 175, 2272-2283.

25. Iwaki, Y.; Yashiro, K.; Kokubo, M.; Mori, T.; Wieting, J. M.; McGowan, K. M.; Bridges, T. M.; Engers, D. W.; Denton, J. S.; Kurata, H.; Lindsley, C. W. Towards a TREK-1/2 (TWIK-Related K^+ Channel 1 and 2) dual activator tool compound: Multi-dimensional optimization of BL-1249. *Bioorg. Med. Chem. Lett.* **2019,** 29, 1601-1604.

26. Vivier, D.; Soussia, I. B.; Rodrigues, N.; Lolignier, S.; Devilliers, M.; Chatelain, F. C.; Prival, L.; Chapuy, E.; Bourdier, G.; Bennis, K.; Lesage, F.; Eschalier, A.; Busserolles, J.; Ducki, S. Development of the first two-pore domain potassium channel TWIK-Related K(+) Channel 1-selective agonist possessing in vivo antinociceptive activity. *J. Med. Chem.* **2017,** 60, 1076-1088.

27. Descoeur, J.; Pereira, V.; Pizzoccaro, A.; Francois, A.; Ling, B.; Maffre, V.; Couette, B.; Busserolles, J.; Courteix, C.; Noel, J.; Lazdunski, M.; Eschalier, A.; Authier, N.; Bourinet, E. Oxaliplatin-induced cold hypersensitivity is due to remodelling of ion channel expression in nociceptors. *EMBO. Mol. Med.* **2011,** 3, 266-278.

28. Busserolles, J.; Tsantoulas, C.; Eschalier, A.; Lopez Garcia, J. A. Potassium channels in neuropathic pain: advances, challenges, and emerging ideas. *Pain* **2016,** 157 Suppl 1, S7-14.

29. Stumpf, F.; Algul, H.; Thoeringer, C. K.; Schmid, R. M.; Wolf, E.; Schneider, M. R.; Dahlhoff, M. Metamizol relieves pain without interfering with cerulein-induced acute pancreatitis in mice. *Pancreas* **2016,** 45, 572-578.

30. Le Guilloux, V.; Schmidtke, P.; Tuffery, P. Fpocket: an open source platform for ligand pocket detection. *BMC. Bioinformatics.* **2009,** 10, 168.

31. Schwartz, E. S.; La, J. H.; Scheff, N. N.; Davis, B. M.; Albers, K. M.; Gebhart, G. F. TRPV1 and TRPA1 antagonists prevent the transition of acute to chronic inflammation and pain in chronic pancreatitis. *J. Neurosci.* **2013,** 33, 5603-5611.

32. Schwartz, E. S.; Christianson, J. A.; Chen, X.; La, J. H.; Davis, B. M.; Albers, K. M.; Gebhart, G. F. Synergistic role of TRPV1 and TRPA1 in pancreatic pain and inflammation. *Gastroenterology* **2011,** 140, 1283-1291.e1-2.

33. Basurto Ona, X.; Rigau Comas, D.; Urrutia, G. Opioids for acute pancreatitis pain. *Cochrane. Database. Syst. Rev.* **2013**, Cd009179.

34. Meng, W.; Yuan, J.; Zhang, C.; Bai, Z.; Zhou, W.; Yan, J.; Li, X. Parenteral analgesics for pain relief in acute pancreatitis: a systematic review. *Pancreatology* **2013,** 13, 201-206.

35. Lerch, M. M.; Gorelick, F. S. Models of acute and chronic pancreatitis. *Gastroenterology* **2013,** 144, 1180-1193.

36. Gerebtzoff, G.; Seelig, A. In silico prediction of blood-brain barrier permeation using the calculated molecular cross-sectional area as main parameter. *J. Chem. Inf. Model.* **2006,** 46, 2638-2650.

37. Laigle, C.; Confort-Gouny, S.; Le Fur, Y.; Cozzone, P. J.; Viola, A. Deletion of TRAAK potassium channel affects brain metabolism and protects against ischemia. *PLoS One* **2012,** 7, e53266.

38. Machelska, H.; Celik, M. O. Advances in achieving opioid analgesia without side effects. *Front. Pharmacol.* **2018,** 9, 1388.

39. Talbot, S.; Abdulnour, R. E.; Burkett, P. R.; Lee, S.; Cronin, S. J.; Pascal, M. A.; Laedermann, C.; Foster, S. L.; Tran, J. V.; Lai, N.; Chiu, I. M.; Ghasemlou, N.; DiBiase, M.; Roberson, D.; Von Hehn, C.; Agac, B.; Haworth, O.; Seki, H.; Penninger, J. M.; Kuchroo, V. K.; Bean, B. P.; Levy, B. D.; Woolf, C. J. Silencing nociceptor neurons reduces allergic airway inflammation. *Neuron* **2015,** 87, 341-354.

40. Jabaudon, M.; Belhadj-Tahar, N.; Rimmele, T.; Joannes-Boyau, O.; Bulyez, S.; Lefrant, J. Y.; Malledant, Y.; Leone, M.; Abback, P. S.; Tamion, F.; Dupont, H.; Lortat-Jacob, B.; Guerci, P.; Kerforne, T.; Cinotti, R.; Jacob, L.; Verdier, P.; Dugernier, T.; Pereira, B.; Constantin, J. M. Thoracic epidural analgesia and mortality in acute pancreatitis: a multicenter propensity analysis. *Crit Care. Med* **2018,** 46, e198-e205.

41. Windisch, O.; Heidegger, C. P.; Giraud, R.; Morel, P.; Buhler, L. Thoracic epidural analgesia: a new approach for the treatment of acute pancreatitis? *Crit Care* **2016,** 20, 116.

42. Dong, Y. Y.; Pike, A. C.; Mackenzie, A.; McClenaghan, C.; Aryal, P.; Dong, L.; Quigley, A.; Grieben, M.; Goubin, S.; Mukhopadhyay, S.; Ruda, G. F.; Clausen, M. V.; Cao, L.; Brennan, P. E.; Burgess-Brown, N. A.; Sansom, M. S.; Tucker, S. J.; Carpenter, E. P. K2P channel gating mechanisms revealed by structures of TREK-2 and a complex with Prozac. *Science* **2015,** 347, 1256-1259.

43. Brohawn, S. G.; Campbell, E. B.; MacKinnon, R. Domain-swapped chain connectivity and gated membrane access in a Fab-mediated crystal of the human TRAAK K+ channel. *Proc. Natl. Acad. Sci. U. S. A.* **2013,** 110, 2129-2134.

44. Brohawn, S. G.; del Marmol, J.; MacKinnon, R. Crystal structure of the human K2P TRAAK, a lipid- and mechano-sensitive K+ ion channel. *Science* **2012,** 335, 436-441.

45. Brohawn, S. G.; Campbell, E. B.; MacKinnon, R. Physical mechanism for gating and mechanosensitivity of the human TRAAK K+ channel. *Nature* **2014,** 516, 126-130.

46. Lolicato, M.; Riegelhaupt, P. M.; Arrigoni, C.; Clark, K. A.; Minor, D. L., Jr. Transmembrane helix straightening and buckling underlies activation of mechanosensitive and thermosensitive K(2P) channels. *Neuron* **2014,** 84, 1198-1212.

47. Davis, I. W.; Baker, D. RosettaLigand docking with full ligand and receptor flexibility. *J. Mol. Biol.* **2009,** 385, 381-392.

48. Lemmon, G.; Meiler, J. Rosetta Ligand docking with flexible XML protocols. *Methods. Mol. Biol.* **2012,** 819, 143-155.

49. Huang, W.; Cane, M. C.; Mukherjee, R.; Szatmary, P.; Zhang, X.; Elliott, V.; Ouyang, Y.; Chvanov, M.; Latawiec, D.; Wen, L.; Booth, D. M.; Haynes, A. C.; Petersen, O. H.; Tepikin, A. V.; Criddle, D. N.; Sutton, R. Caffeine protects against experimental acute pancreatitis by inhibition of inositol 1,4,5-trisphosphate receptor-mediated Ca2+ release. *Gut* **2017,** 66, 301-313.

50. Huang, W.; Booth, D. M.; Cane, M. C.; Chvanov, M.; Javed, M. A.; Elliott, V. L.; Armstrong, J. A.; Dingsdale, H.; Cash, N.; Li, Y.; Greenhalf, W.; Mukherjee, R.; Kaphalia, B. S.; Jaffar, M.; Petersen, O. H.; Tepikin, A. V.; Sutton, R.; Criddle, D. N. Fatty acid ethyl ester synthase inhibition ameliorates ethanol-induced Ca2+-dependent mitochondrial dysfunction and acute pancreatitis. *Gut* **2014,** 63, 1313-1324.

Table of Contents graphic